THE LANCET
Public Health

Supplementary appendix

This appendix formed part of the original submission and has been peer reviewed. We post it as supplied by the authors.

Supplement to: Masters NB, Beck AS, Mathis AD, et al. Measles virus transmission patterns and public health responses during Operation Allies Welcome: a descriptive epidemiological study. *Lancet Public Health* 2023; **8:** e618–28.

Supplementary Appendix

This appendix has been provided by the authors to give readers additional information about their work.

Supplement to: Masters NB, Beck AS, Mathis AD, et al. Measles virus transmission patterns and public health responses during Operation Allies Welcome: a descriptive epidemiological study

Table of Contents

Supplementary Methods

List of Figures

List of Tables

Laboratory confirmation of measles cases

Laboratory confirmation included the detection of measles-specific IgM in serum by enzyme immunoassays or the detection of measles virus RNA in a nasopharyngeal or urine specimen by real-time reverse-transcription–polymerase-chain-reaction (RT–PCR) assays, or both. Assays to detect IgM were performed at commercial laboratories, the Virginia Division of Consolidated Laboratory Services (DCLS), and CDC. Detection of measles virus RNA was performed at the Virginia DCLS, New York State Public Health Laboratory (NY), Wisconsin State Public Health Laboratory (WI), CDC, and California State Public Health Laboratory (CA). Measles genotyping and an RT-PCR assay to detect the measles vaccine strain (MeVA) [1] were performed in WI, NY, CA, and CDC.

Measles Mumps Rubella (MMR) vaccine uptake

Rates of MMR vaccine uptake among eligible Afghan evacuees during OAW were calculated using US Department of Defense (DoD) data reports documenting the daily and cumulative number of MMR doses administered at each military base from September 9 to October 15, 2021. DoD reports were available for 30 of the 37 days covering this period. To impute the number of MMR doses administered in days with missing data (October 3–7 and October 9–10) we calculated the difference in cumulative MMR doses across the data gap and assumed the doses were evenly distributed among missing days.

DoD started reporting the daily and cumulative number of MMR doses administered at each military base on September 9, 2021. Limited vaccination of arriving Afghan evacuees occurred as early as August 24, 2021. We assumed the cumulative number of MMR doses documented in the September 9 report to be evenly distributed from August 24–September 8, 2021.

Rates of MMR vaccine uptake at Hotel A were calculated using Department of Homeland Security data on the daily number of MMR doses administered at Hotel A.

MMR vaccine eligibility and estimation of vaccine coverage

Afghan evacuees were considered ineligible for vaccination if they were aged <6 months or pregnant. To estimate the denominator of MMR vaccine eligible evacuees we used three sources of information:

1. Base-specific populations on September 24, 2021, as provided by DoD (below). September 24 was selected because it occurred during the international flight pause and military base quarantine periods, during which base populations were stable.

Populations at eight locations housing Afghan evacuees during Operation Allies Welcome on September 24, 2021.

Location	No. of Arrived Evacuees as of Sep 24, 2021
Camp Atterbury	6,628
Joint Base McGuire-Dix-Lakehurst	9,469
Marine Corps Base Quantico	3,745
Fort Lee	2,583
Fort McCoy	12,833
Fort Bliss	9,977
Fort Pickett	5,988
Holloman Air Force Base	3,916
Hotel A[a]	540
Total	55,679

[a]Contracted isolation and quarantine hotel in Virginia.

2. Proportion of the population aged <6 months. The age distribution of the population in Afghanistan in 2021 were drawn from the United Nations Department of Economic and Social Affairs, Population Division (available here: https://population.un.org/wpp/Download/Standard/CSV/). The proportion of the population aged <6 months (1·7%) was compared to known population distributions available for Hotel A (1.9%) and MCB Quantico (2·0%), and the median of these population proportions (1·9%) was applied to base-specific populations to characterize the number of infants aged <6 months.

3. Number of pregnant women at each base as of October 2, 2021 as provided by DoD. Women of child-bearing age (aged 12–50 years) were screened for pregnancy during the mass MMR vaccination campaigns to assess for vaccine eligibility and to facilitate early prenatal care.

Location-specific populations of pregnant women during Operation Allies Welcome as of October 2, 2021.

Base	No. of Pregnant Women
Camp Atterbury	160
Joint Base McGuire-Dix-Lakehurst	427
Marine Corps Base Quantico	118
Fort Lee	76
Fort McCoy	232
Fort Bliss	117
Fort Pickett	191
Holloman Air Force Base	91
Hotel A[a]	16
Total	1428

[a]Hotel A, the contracted isolation and quarantine hotel in Virginia, was managed by the Department of Homeland Security (DHS) and thus the census of pregnant women was taken over the duration of Hotel A being open to evacuees.

The number of immunocompromised persons was not accounted for in the calculation of the vaccine-eligible population as this information was not available. Rates of MMR vaccine uptake among eligible Afghan evacuees at each location during the pause of international flights is shown below.

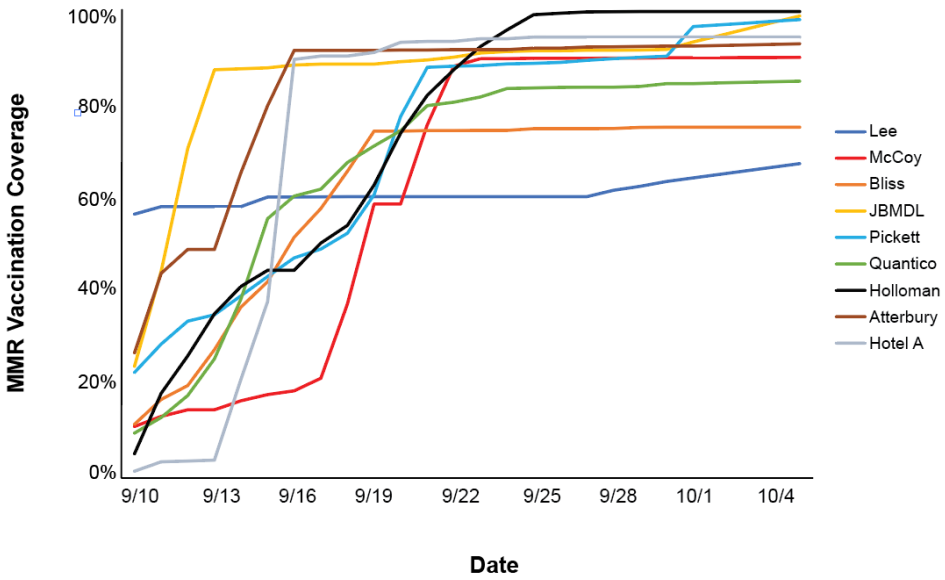

One-dose MMR vaccine uptake among eligible Afghan evacuees by location. One-dose MMR vaccine uptake is plotted across nine military bases and the isolation and quarantine hotel (Hotel A) during the pause on international flights from September 10, 2021 to October 5, 2021.

Model structure and parameterization

The susceptible-exposed-infectious-recovered or *SEIR* model tracks 4 classes of persons: those who are (1) susceptible to infection and disease (*S*); (2) exposed but not yet infectious and asymptomatic (*E*); (3) infectious with symptoms (*I*); and (4) recovered and immune (*R*).

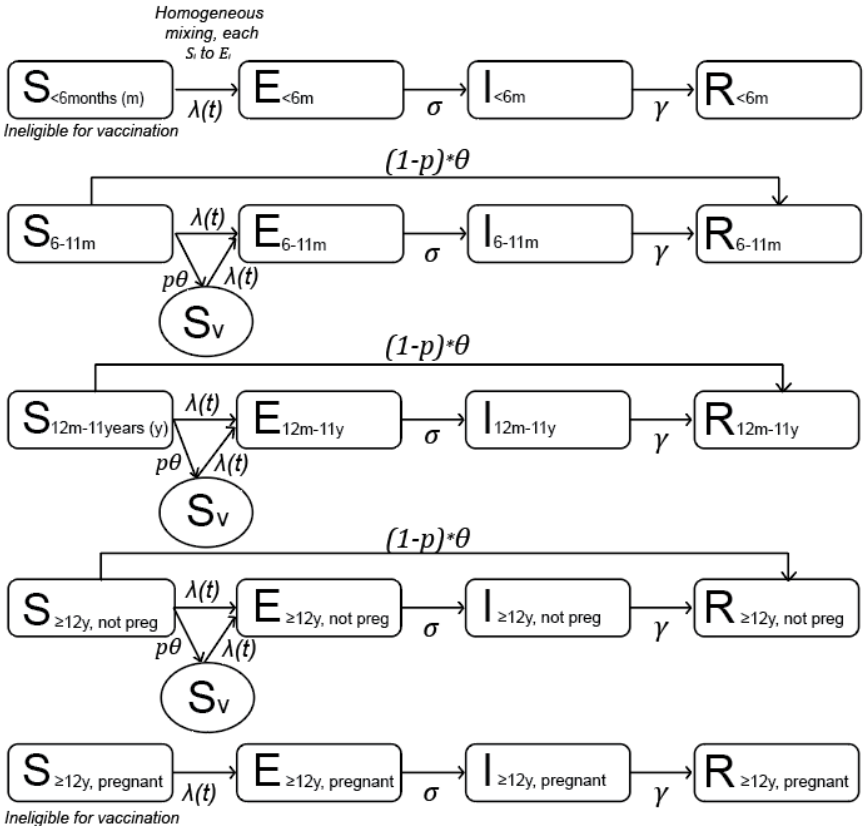

Schematic representation of disease states, flow between states, and parameters controlling flow in a model of measles transmission during Operation Allies Welcome. The model represents a constant (closed) population in which individuals belong to one of four states related to measles infection: susceptible (*S*), exposed (*E*), infected (*I*), and recovered (*R*). The model tracks the daily number of persons in each compartment, and incorporates stochasticity using the adaptive tau-leaping algorithm.[2,3] Individuals in the susceptible pool (*S*) become exposed by the force of infection $\lambda(t) = \beta * I_t$, the per capita rate at which 2 persons come into sufficient contact to lead to infection per unit of time (β) times the number of infectious persons at time t (I_t), and progress to the exposed preinfectious (*E*) state. Transitions into the *I* and *R* compartments are determined by rates σ and γ, respectively. The effect of mass measles-mumps-rubella (MMR) vaccination is denoted by θ; susceptible persons are removed from the *S* compartment and added to the *R* compartment based on the date MMR vaccine was administered, with a lag-time of 7 days to account for a delay in vaccine-induced immunity. The compartment S_v pertains to individuals who were vaccinated and failed to produce an adequate immune response (primary vaccine failures). *p* represents the probability of primary vaccine failure (or 1–vaccine effectiveness).

Transitions from the *S* to *I* compartments are determined by the transmission rate β (the per capita rate at which two persons come into sufficient contact to lead to infection per unit of time) and to the number of infectious persons at time t (I_t). β can be calculated as $\frac{R_0}{ND}$ where R_0 is the basic reproduction number, or average number of secondary cases generated per infected individual in a fully susceptible population, *N* is the population size, and *D* is the duration of infectiousness.

R_0 in a particular population can be derived from the effective reproduction number R_e,or average number of secondary cases generated per infected individual in a population with some level of immunity, and the proportion of the population susceptible *s*, as $R_0 = \frac{R_e}{s}$.

We adapted[4] the Wallinga and Teunis algorithm,[5,6] a maximum likelihood approach that uses the time between illness onset of cases in the same infection cluster and the probability density of the serial interval (time between the successive illness onsets in a transmission chain), to infer R_e. We used dates of rash onset

and a serial interval derived from household transmission studies with a gamma probability distribution and a mean (standard deviation) of 11·1 (2·47) days. [7]

To obtain a range of $R_e$values, we applied the algorithm to observed measles patients in the following settings: (1) all locations; (2) Ft. McCoy; and (3) a single barrack with a high attack rate at Fort McCoy, Barrack A. The first was selected because many patients shared the same itineraries to come to the U.S. and could have been part of a larger infectious cluster. The second and third were selected because these were more defined infection clusters. To calculate R_o, we used early estimates of R_e that would be less affected by the containment measures implemented across bases, particularly the rapid rise in vaccine uptake, and reflect more baseline population immunity.

To estimate the proportion of the population that was susceptible at the outset, we developed an age-specific immunity profile of Afghanistan in 2021 based on routine immunization coverage and supplementary immunization activities (details provided below). We used a weighted average of age-specific immunity estimates (weighted by population size within each age-stratum) to inform overall susceptibility and to derive R_0 from R_e. Resulting R_0 estimates are shown below; these were consistent with prior R_0 estimates of measles in various settings (range, 5–18). [8,9] We used the median value of R_0, 14·00, for primary analyses. Because of the uncertainty around baseline immunity levels in this population (see below) and several caveats that could affect estimation of R_e (e.g., not being able to fully account for importations and use of prior estimates of the serial interval), [10] sensitivity analyses were performed around the estimated R_0 values.

R_e estimates based on the Wallinga-Teunis method by setting and R_o derivations

Setting	R_e*	Proportion susceptible *s*	R_0§
1) All locations	2·46	17·57%	14·00
2) Ft. McCoy	2·03		11·55
3) Barrack A at Ft. McCoy	2·67		15·20

*Early estimates of R_e for all locations, Ft. McCoy, and Barrack A were obtained during 7-day windows ending on transmission day 8, 11, and 8, respectively.
§Calculated as R_e/s

The infectiousness rate σ and the recovery rate γ describe the rates at which individuals progress into the *I* and *R* compartments and are inversely proportional to the pre-infectious period (the time period between infection and onset of infectiousness) and the duration of infectiousness, respectively. We parameterized the model using an 8-day pre-infectious period and a 5-day duration of infectiousness. [11,12]

In the model, evacuees susceptible to measles who received MMR vaccine are removed from the *S* compartment and added to the *R* compartment according to the date of vaccine receipt and assuming a 7-day delay in acquisition of vaccine-derived immunity. We assumed a vaccine effectiveness (VE) of one-dose of MMR vaccine to be 84% for infants aged 6–11 months and 92·5% for persons aged ≧12 months. [13,14] For each stratum, we created an additional compartment, S_v, for once-vaccinated evacuees who remained susceptible (primary vaccine failure) and who could contribute to transmission, but who were not vaccinated a second time during initial mass vaccination campaigns.

The differential equations *approximating* the stochastic process of this model are listed below, with state variables (e.g. S_i, E_i) representing proportions of the total population:

$$\frac{dS_i(t)}{dt} = -\beta I(t) S_i(t) - \theta(t) S_i(t)$$

$$\frac{dS_{v_i}(t)}{dt} = p * \theta(t) S_{v_i}(t) - \beta I(t) S_{v_i}(t)$$

$$\frac{dE_i(t)}{dt} = \beta I(t) S_i(t) + \beta I(t) S_{v_i}(t) - \sigma E_i(t)$$

$$\frac{dI_i(t)}{dt} = \sigma E_i(t) - \gamma I_i(t)$$

$$\frac{dR_i(t)}{dt} = \gamma I_i(t) + (1-p) * \theta(t) S_i(t)$$

$$\text{where } I(t) = \sum_{i=1} I_i(t) \text{ and the force of infection, } \lambda(t) = \beta I(t)$$

The model was divided into five strata based on MMR vaccine eligibility: (1) <6 months of age; (2) 6–11 months of age; (3) 1–11 years of age; 4) ≥12 years of age and not pregnant; and (5) ≥12 years of age and pregnant. We assumed homogeneous mixing between strata due to the congregate living environment of evacuees across the bases, where families of mixed ages resided in barracks, and all ages intermixed at common facilities such as dining and recreation areas. We used finite population sizes for each base based on the population denominators from September 24, 2021. Models were run 1000 times for 200 days independently at each of the five bases that reported cases. Models were started with one importation each into Ft. McCoy, MCB Quantico, Ft. Pickett, and JBMDL, and two importations into Holloman Air Force Base, based on the minimum number of potential importations (Figure 4). In certain outbreaks in the U.S., as was the case during OAW, some cases that are classified as an international importation (i.e. if at least some of the patient's exposure period (7–21 days before rash onset) occurred outside the U.S. and rash onset occurred within 21 days of entering the U.S., with no known measles exposure in the U.S. during that time), might actually be secondary cases to a first importation, because the link or exposure between these cases cannot be verified. This can occur when there are multiple importations and considerable mixing in the affected population. Because the probability of an outbreak and the number of subsequent cases increases with an increase in the number of importations, to initiate the models, we conservatively assumed the minimum number of importations that could explain subsequent cases at each of the bases.

Modeling the vaccination campaigns

The number of daily MMR doses administered at each of the affected bases and Hotel A were used to model the vaccination campaigns. MMR vaccine was administered to all eligible individuals who lacked written documentation of MMR vaccination. Because availability of vaccination records among evacuees was exceptionally rare, doses were given indiscriminately during the vaccination campaigns, including to those who may have been already immune from prior vaccination or natural disease but who lacked such documentation. Thus, we proportioned the daily doses of MMR among evacuees who were eligible to be vaccinated (i.e., those in strata 2, 3, and 4), based on the proportion these groups contributed to in terms of overall population size at each base.

Calculation of susceptibility profile

Because of maternal or natural immunity, or prior vaccination, the model assumes a proportion of the population is in the recovered compartment at the outset. Serosurveys that characterize the immunity profile in Afghanistan are unavailable. We estimated the age-specific measles immunity profile of Afghanistan in 2021 using an approach described by Xi Li, Robert Perry, and James Goodson at the WHO Meeting of the Advisory Committee on Immunization and Vaccine related Implementation Research. [15] The approach estimates age-specific immunity levels reached through routine immunization with the first (MCV1) and second (MCV2) dose of a measles-containing vaccine, as well as through supplementary immunization activities (SIAs).

Routine immunization coverage data for MCV1 and MCV2 were obtained from WHO/UNICEF Joint Estimates of National Immunization Coverage (WUENIC) (https://immunizationdata.who.int) and SIA coverage data were obtained from WHO/IVB Database of SIAs (https://immunizationdata.who.int/listing.html?topic=additional-data&location=). The total population in Afghanistan in 2021 by single age groups were drawn from the United Nations Department of Economic and Social Affairs, Population Division (https://population.un.org/wpp/Download/Standard/CSV/). All sites were accessed on July 14, 2022.

In this approach it is assumed that previously vaccinated children are reached first for a subsequent vaccine dose (either through MCV2 or SIA) before unvaccinated children ("dependent scenario"). [15] The following formulas were used to estimate age-specific immunity levels, with equations 2 and 3 applied incrementally to the prior equation, such that, for example, equation 2 is applied to those who have been vaccinated with MCV1:

(1) $\%\ of\ persons\ immune\ from\ MCV1 = Coverage_{MCV1} * VE_{MCV1}$

(2) $\%\ of\ additional\ persons\ immune\ from\ MCV2$

$$= (Coverage_{MCV1} - Coverage_{MCV1} * VE_{MCV1}) * \frac{Coverage_{MCV2}}{Coverage_{MCV1}} * VE_{MCV2}$$

(3) $\%\ of\ additional\ persons\ immune\ from\ SIA_n$

$$= \begin{cases} (cum_{vax} - cum_{immune}\ ) * \dfrac{Coverage_{SIA_n}}{cum_{vax}} * VE_{SIA} * \%\ population\ targeted, \\ \qquad when\ SIA_n\ coverage < cum_{vax} \\ \\ \left(Coverage_{SIA_n} - cum_{immune}\right) * VE_{SIA} * \%\ population\ targeted,\ \ when\ SIA_n \geq cum_{vax} \end{cases}$$

$$cum_{vax} = \ cumulative\ \%\ vaccinated\ before\ SIA_n$$
$$cum_{immune} = \ cumulative\ \%\ immune\ before\ SIA_n$$

In Afghanistan, MCV1 is recommended at 9 months for age, and MCV2 is recommended at 18 months of age. [16] VE for MCV1 was assumed to be 84·0% when received at 6–11 months of age and 92·5% when received at ≥12 months of age. [14] VE for MCV2 was assumed to be 95%. For the SIAs, the corresponding VE was applied based on the age cohorts targeted by the particular SIA and whether prior doses were received. [15]

Available SIA coverage was based on administrative data, which can be biased because of inaccurate numerators or denominators. Because 12 (close to two-thirds) of the 19 SIA coverage estimates were >95%, including 8 estimates >100%, we adjusted all SIA estimates by a factor of 81% based on a single available post-campaign assessment showing a coverage of 92% for an SIA with reported administrative coverage of 113%. Derived estimates of age-specific immunity and susceptibility in Afghanistan are shown below.

Age-specific estimates of measles immunity and susceptibility in Afghanistan

Birth year	Age*	% immune by MCV1	% immune by MCV2**	% immune by SIAs^	% immune by maternal antibody	% susceptible
2021	0–5 months‡	0·00	0·00	0·00	66·67	33·33
2021	6–11 months‡‡	26·46	0·00	0·00	33·33	40·21
2020	1	55·44	6·69	0·00	0·00	37·87
2019	2	53·76	6·54	0·00	0·00	39·70
2018	3	59·64	6·23	1·25	0·00	32·88
2017	4	56·28	7·45	10·35	0·00	25·92
2016	5	53·76	6·08	14·23	0·00	25·93
2015	6	52·08	6·08	16·18	0·00	25·66
2014	7	50·40	6·38	34·81	0·00	8·40
2013	8	47·88	6·69	37·04	0·00	8·39
2012	9	49·56	5·78	36·24	0·00	8·42
2011	10	53·76	5·02	33·06	0·00	8·16
2010	11	52·08	4·71	26·01	0·00	17·20
2009	12	50·40	4·41	27·76	0·00	17·43
2008	13	49·56	3·65	40·55	0·00	6·24
2007	14	46·20	3·50	43·41	0·00	6·89
2006	15	44·52	0·61	37·02	0·00	17·85
2005	16	42·00	2·74	41·28	0·00	13·98
2004	17	40·32	1·37	44·01	0·00	14·30
2003	18	32·76	0·30	51·61	0·00	15·33
2002	19	29·40	0·00	59·62	0·00	10·98
2001	20	31·08	0·00	45·72	0·00	23·20
2000	21	22·68	0·00	53·92	0·00	23·40
1999	22	26·04	0·00	50·58	0·00	23·38
≤1998	23–100+	–	–	–	–	12·00*****

[*]Age is presented in years unless otherwise specified.
[**]MCV2 was introduced in Afghanistan in 2004.
[^]Because 12 (close to two-thirds) of the 19 SIA coverage estimates were above 95%, including 8 estimates above 100%, we adjusted these estimates by a factor of 81% based on a single available post-campaign assessment showing a coverage of 92% for an SIA reporting a coverage of 113% based on administrative data.
[ǂ]Infants were divided into two age-groups (<6 months and 6–11 months of age) based on our model strata. Because MCV1 is given starting at 9 months of age, half of the MCV1 coverage reported in 2021 was applied to infants aged 6–11 months. Maternally derived measles immunity among infants was assumed to be 50% (66·67% of infants aged <6 months and 33·33% of infants aged 6–11 months were assumed to be immune). [17]
[#]Based on data from Freidl et al. showing 88% of adult Afghan asylum seekers born between 1998 and 1971 in the Netherlands were seropositive for measles. [18]

Stratification of the model and age dependent susceptibilities

The model is divided into five strata according to MMR vaccine eligibility, i.e., based on four age groups (<6 months of age, 6–11 months of age, 12 months–11 years of age, and ≥12 years of age) and pregnancy status (≥12 years of age and not pregnant and ≥12 years of age and pregnant). Complete information on the age distribution of Afghan evacuees were available for MCB Quantico and Hotel A; these distributions were similar to the age distribution of the population in Afghanistan in 2021, below. We applied the median of these proportions to base-specific populations to determine age-specific subpopulations for the stratified model. The number of pregnant women at each base as of October 2, 2021 was used to inform the last stratum (≥12 years of age and pregnant).

Proportion of Afghan evacuees in each of four age groups based on three different data sources and median values used for vaccine-eligibility calculations, derivation of age-specific populations for the simulation analyses, and estimation of overall susceptibility.

Age group	Data Source			Median values used in analyses
	UN Department of Economic and Social Affairs, Population Division	Hotel A	MCB Quantico	
<6 months	1·7%	1·9%	2·0%	1·9%
6–11 months	1·7%	1·5%	1·4%	1·5%
1–11 years	32·5%	39·0%	37·7%	37·7%
≥12 years	64·1%	57·0%	58·9%	58·9%

The measles immunity profile of Afghanistan was used to generate weighted averages of initial susceptibility in each of our four age strata (<6 months, 6–11 months, 1–11 years, ≥12 years), i.e., for age strata spanning more than a single age year (age strata 1–11 years and ≥12 years), the overall susceptibility of the particular strata was the weighted average of the susceptibility based on the relative population size of the single age years within the age strata, as below.

Proportions of the population estimated to be susceptible to measles in each of four age groups.

Age Group	Weighted Susceptibility (%)
<6 months[*]	33·33
6–11 months[*]	40·21
1–11 years	22·47
≥12 years	13·35

[*]Because the number of birth cohorts included in the infant age categories do not span more than 1 year, the susceptibility of infants aged <6 months and 6–11 months is not weighted.

Calculation of overall susceptibility of Afghan evacuees to derive R_0 from R_e

Similarly, the overall susceptibility of Afghan evacuees (across all ages) used to derive R_0 from R_e was calculated as the weighted average (weighted by population size within each age-stratum) of age group-specific immunity estimates, as follows:

$$Overall\ Susceptibility = proportion_{<6m} * susceptibility_{<6m} + proportion_{6-11m} * susceptibility_{6-11m} + proportion_{12m-11y} * susceptibility_{12m-11y} + proportion_{\geq 12y} * susceptibility_{\geq 12y}$$

Limitations of measles immunity profile of Afghanistan

Several limitations to the approach used to estimate the immunity profile of Afghanistan should be considered. First, the approach does not incorporate immunity derived from natural infection, and it could underestimate overall population immunity, particularly among older age groups who were born when measles coverage was low, and levels of measles circulation were high. Second, the approach does not account for heterogeneity in vaccine coverage and assumes measles vaccine doses administered both routinely and through supplementary immunization activities (SIAs) were distributed homogenously across subpopulations. Third, among older age-groups, for whom measles vaccination or measles vaccination coverage estimates were unavailable, we used published data on measles immunity levels among adult Afghan asylum seekers in The Netherlands, [18] which might not be generalizable to the evacuee population of OAW. Finally, the precision of the profile estimates relies on the accuracy of the data on routine immunization and SIA coverage. For routine immunization, we used WHO and UNICEF estimates of national immunization coverage which are more conservative than coverage estimates based on administrative data. SIA coverage was based on administrative data, which can under- or overestimate vaccination coverage. Because post-campaign coverage surveys were unavailable, we adjusted the reported SIA coverage by 81% based on a single post-campaign assessment.

Although representative age-specific measles seroprevalence data are not available for Afghanistan, we were able to benchmark our estimates with serology data obtained from a subset of Afghan evacuees at Ft. McCoy. These individuals were potentially exposed to the first measles case identified at Ft. McCoy and included all co-passengers on the same flight arriving to Ft. McCoy from Dulles International Airport, as well as the flights before and after the first case's flight (due to overlapping times at Dulles International Airport and during intake at Ft. McCoy). Testing was done using an enzyme immunoassay through a U.S. commercial laboratory. This test is calibrated against the established correlate of protection of 120 mIU/ml by the plaque reduction neutralization (PRN) assay. Among these 441 Afghan evacuees at Ft. McCoy tested using an enzyme immunoassay, measles-specific IgG antibodies were positive in 208 evacuees, negative in 107 evacuees, and equivocal in 126 evacuees. The overall proportion susceptible based on negative results alone was 24·2%, suggesting the approach we used might be underestimating overall susceptibility. Below, we show the IgG antibody results by age group:

Seroprevalence data from a subset of Afghan evacuees at Ft. McCoy tested for measles IgG with a commercial enzyme immunoassay

Test result	Age group	Percent
	<6 months	
Positive	2	18%
Negative	2	18%
Equivocal	7	64%
Total	11	-
	6–12 months	
Positive	1	14%
Negative	2	29%
Equivocal	4	57%
Total	7	-
	12 months–12 years	
Positive	59	40%
Negative	46	31%
Equivocal	43	29%
Total	148	-
	≥12 years	
Positive	141	53%
Negative	52	20%
Equivocal	71	27%
Total	264	-

Because of these important caveats, the model trajectories we present are not intended to be exact projections, but rather serve to characterize relative differences in transmissibility under various scenarios in order to assess the impact of public health interventions. In addition, sensitivity analyses were performed around estimated susceptibility levels.

Modeling measles transmission at Hotel A

Using the approach described above, we also modeled potential outbreak trajectories at the isolation and quarantine hotel (Hotel A) in Virginia. Because of a few key differences between Hotel A and the military bases, results from this analysis are reported separately and were not incorporated into pooled results in the main text. As a contracted isolation and quarantine facility, Hotel A received Afghan evacuees who had (or were exposed to) certain infectious diseases, including patients suspected of having measles. Evacuees noted to have symptoms (e.g., fever, rash) at Dulles International Airport were either transported to the hospital directly for medical assistance and evaluation, and upon discharge, went to Hotel A, or were transported directly to Hotel A with their family unit. Because suspected measles patients identified upon arrival to the United States were referred to Hotel A, Hotel A had substantially more importations compared to other settings (Figure 2). Social contacts and mixing in Hotel A might have been different to that seen at military bases, as patients with different conditions or exposures were grouped together on different floors. Hotel A also had a much smaller population compared to the military bases. Finally, isolation and quarantining at Hotel A ceased after about two months from the initiation of OAW, and thus measles transmission was modeled over a different time frame. We modeled measles transmission at Hotel A starting with 4 importations for a period of 60 days.

Sequencing and Phylogenetic Analyses

Genotyping by Partial Sequence Window (N450)

N450 genotyping was performed at CDC and the Wisconsin State Laboratory of Hygiene. The N450 fragment is obtained from the C-terminal 450 bases of the measles virus nucleoprotein gene (excluding the terminal stop codon), the analyses of which is widespread in molecular surveillance practice. [19] Briefly, total nucleic acids (TNA) were extracted from clinical specimens (nasopharyngeal/oropharyngeal swabs); 5µL of TNA was subjected to reverse-transcription PCR (RT-PCR) amplification. Amplicons were column-purified and sequenced to double-per-reaction coverage by Sanger chemistry. Contigs were assembled, quality-edited, and then trimmed again to produce the final N450 window. Resulting N450 contigs were aligned to WHO standards to ascertain genotype (B3 for all specimens). During Operation Allies Welcome, 8 measles vaccine reactions were identified by detection of measles genotype A or a vaccine-specific RT-PCR assay (MeVa).

Preparation of Unbiased RNA-Seq Libraries to Obtain Whole Genomes

20µL of specimen extract (total nucleic acid) was digested with RNAse-free DNAse for 10min at 37ºC (NEB, Ipswich, MA). RNA-Seq libraries were prepared using non-directional NEBNext® chemistry (NEB) according to manufacturer's instructions, with the following modifications: (1) RNA fragmentation was performed for 7min30s at 94ºC. (2) First strand synthesis was performed according to long-fragment recommendations – (10min at 25ºC, 50min at 42ºC, 15min at 70ºC). (3) At ligation, adaptors were diluted to a ratio of 1:100. (4) Indexing PCR was performed using recommended cycling parameters in the presence of unique dual index (UDI) oligos (NEB), for 20 cycles. Final library size distribution was confirmed using Tapestation® high-sensitivity D1000 capillary electrophoresis (Agilent, Santa Clara, CA). Library concentrations were verified by real-time PCR targeting Illumina adaptor ends (NEB).

Enrichment of Measles cDNA Fragments in Illumina RNA-Seq Libraries to Improve Assembly

Libraries were enriched for measles virus fragments using a modification of the probe-hybridization method of Metsky (CATCH). [20] Briefly, 2µL of cDNA library was hybridized to biotin-tagged RNA probes in the presence of adaptor blocking primers, Human Cot-1 DNA, and sheared salmon sperm DNA for 4h at 65ºC. Probe-fragment hybrids were bound to MyOne® C1 magnetic, streptavidin-coated beads (Invitrogen/Fisher) and then washed 3x in the presence of buffers containing SSC solution and 10% SDS. Purified library was denatured from beads with 0.1 N NaOH, and was amplified using 0.1uM P5/P7 universal primers in the presence of Phusion® (NEB) G-C buffered master mix (NEB). Amplification program was as follows: Initial denaturation at 95ºC for 30s, 30 cycles of denaturation (10s, 95ºC), annealing (30s, 55ºC) and extension (30s, 72ºC). Final extension was for 5min at 72ºC. In all cases, cDNA libraries were purified using SPRISelect® magnetic beads (Beckman, Indianapolis, IN). Library size distribution and concentration were determined as

described above before normalization and sequencing. Files containing primer/probe design are available at study repository: https://data.cdc.gov/Models/Measles-Case-and-Genetic-Metadata-Operation-Allies/b8tp-jsmh.

WGS Quality Control and Assembly to Produce Consensus Sequences

Paired-end read sets were concatenated from separate sequencer lanes and were adaptor and quality-trimmed using Trimmomatic v.0.39, using a sliding window of four bases and an average quality cutoff of 15; retained reads below 20 bases in remaining length were discarded. Trimmed reads (paired and singlet) reads were assembled *de novo* using SPAdes v.3.15.4. Contigs were aligned to reference sequence AF266287 (measles genotype A) using Mummer (nucmer) 4.0.0, and a preliminary *de novo* scaffold was generated using the assembly.py order_and_orient utility of *viral-ngs*. A more comprehensive alignment scaffold incorporating reference bases was then generated using the assembly.py impute_from_reference utility of *viral-ngs*. Trimmed read sets were realigned to this preliminary scaffold using Bowtie v.2.4.5 under "–very-sensitive-local" presets, then sorted using PicardTools SortSam v.2.5 and deduplicated using PicardTools MarkDuplicates v.2.5. Two local indel realignment passes were performed using RealignerTargetCreator and IndelRealigner utilities of GATK v.3.7. Consensus bases were called from refined alignments using the UnifiedGenotyper in GATK v.3.7, producing consensus calls for any available pileup majority (base/indel) observed from a minimum of 10x read coverage. While covered at below a depth of 10 reads, two specimens (MVs/Wisconsin.USA/37.21/4 and MVs/Wisconsin.USA/38.21) contained small regions of base ambiguity in the MF-NCR region, and Sanger contigs were generated directly from specimen TNA extracts to supply those base calls. Final annotations for NCBI submission were performed using VADR v.1.4.1. Human read content was stripped using Kraken 2 before upload of untrimmed fastqs to SRA. Sequence assembly pipeline was documented and controlled using Snakemake v.7.3.0, pipeline is available from the authors in this format or at the manuscript data repository: https://data.cdc.gov/Models/Measles-Case-and-Genetic-Metadata-Operation-Allies/b8tp-jsmh. Illumina reads, consensus assemblies, and Sanger contigs are contained in NCBI Bioproject PRJNA869081.

Common Phylogenetic and Graphical Methods (WGS and N450)

Public repository sequences were downloaded from NCBI on May 03, 2022, searching for the terms "Measles Virus Genotype B3"; sequences were excluded if the N-L span was not represented, if degenerate bases were present, if the sequence was tagged as a vaccine, isolated, laboratory-adapted, or obtained from an encephalitic measles disease process (e.g. measles inclusion body encephalitis (MIBE), subacute sclerosing panencephalitis (SSPE)). Sequences were aligned using MAFFT v.7.4.1, and suitability of alignment was visually inspected. Public repository accessions for sequences and sequencing data used in phylogenetic analyses is available in the study data repository at https://data.cdc.gov/Models/Measles-Case-and-Genetic-Metadata-Operation-Allies/b8tp-jsmh. The resulting alignment was prepared alongside reasonable tip dates for the taxa represented, which for publicly available sequences is the date of the centroid (Thursday) for the epidemiological week shown in WHO nomenclature. For sequences newly obtained in this study, the rash date was used. Bayesian inference was performed using BEAST v.2.6.3[21]. In all cases, sampling runs were performed using a 200 million step chain, comprised of four independently sampled chains of 50 million steps apiece. Samples were drawn at 10,000-step intervals (20,000 trees per run in total for each experiment). 10 percent burn in was discarded. Also in all cases, a Bayesian skyline coalescent tree prior was used, [22] with default pop.sizes=5 and group.sizes=5. A maximum clade credibility tree was prepared from the best-fit model using mean node heights and then annotated with case metadata using R v.4.1.2 with ggtree v.3.0.4 and treeio v.1.16.2.

Specific Phylogenetic Methods (WGS)

Base substitution models were selected using the modeltest function of IQ-Tree v.2.1.2, [23] using separate input partitions for (1) a concatenation of all individual coding sequence regions (CDS) and (2) a concatenation of all intergenic regions (NCR). The alignment was limited to the extrema of the nucleoprotein (N) and large (L) protein gene cassettes (N-L span or WGS-t) to prevent use of end artifacts (exclusion of header and trailer). Recommended base substitution models were TIM+F+G4 for concatenated CDSs, and TIM3+F+G4 for concatenated NCRs (BIC score: 58886·030 in aggregate). These base substitution models were used in all later analysis.

Bayesian inference was performed using BEAST v.2.6.3, [21] using a modification of the recommended partitioning scheme from previous tests. In this case, a concatenation of CDS was used as previously

described, but all noncoding content in the N-L span was concatenated and considered simultaneously. Molecular clock models were compared for suitability using the nested sampling[24] technique to determine marginal likelihoods and Bayes factor comparison of fit. In all cases, nested sampling runs were performed as 32 independent runs, each using one particle, subchain length=10,000 and epsilon=1·0 x 10^6.

Fit and suitability of molecular clock models for Bayesian phylogenetic inference.

Data are derived from nested sampling estimates of marginal likelihood, from which Bayes factor differences are calculated from the model of least-adequate fit, considering standard deviations. In all cases, base substitution models are unlinked (considered separately) across partitions. However, there was considerable difficulty in achieving model convergence for models in which the CDS and NCR partition clocks were unlinked. Considering this, it was interpreted that NCR partitions in the data set lacked sufficient clocklikeness to provide stable posterior estimates under either strict or relaxed-clock conditions. The model selected for final presentation was one in which CDS and NCR partitions both used unlinked base substitution models as described above, alongside a linked, strict clock model for CDS and NCR partitions (Marginal likelihood = -29233·742, S.D.= 3·498). Considering these results, the best-fit, partition-linked clock model was used for all Bayesian inference in the study (highlighted in grey, table below).

Clock Type by Partition	CDS/NCRs Linked	Marginal Likelihood	SD	Information	Max ESS	BF from Worst Fit
Exponential (Both)	Linked	-29351·615	3·955	539·409	1264·116	0
Lognormal (Both)	Linked	-29346·465	3·975	499·768	1007·345	5·150
Strict (Both)	Linked	-29233·742	3·498	408·759	1244·604	117·873
Strict(CDS), Exponential(NCR)	Unlinked	-29213·957	3·912	475·329	1295·859	137·658
Strict(CDS), Lognormal(NCR)	Unlinked	-29208·635	3·731	464·290	1023·169	142·980
Strict(CDS), Strict(NCR)	Unlinked	-29186·822	3·840	445·222	913·276	164·793

Specific Phylogenetic Methods (N450)

N450 sequence windows were obtained by RT-PCR and Sanger chemistry when specimen genotyping was originally performed. WGS consensus contigs (previously described) were individually aligned to corresponding Sanger fragments to ascertain divergence of N450 from WGS, if any. Two sequences were available for case 16 (nasopharyngeal and oropharyngeal swab) and were identical; MVs/Wisconsin.USA/39.21/8/1 was retained for analyses while MVs/Wisconsin.USA/39.21/8/2 was excluded from tree inference as a case duplicate. All N450 sequences (n=44 N450 sequences from 43 sequenced cases, 43 sequences used after duplicate exclusion) were identical to corresponding windows assembled by WGS, if available (n=42 WGS sequences from 43 sequenced cases, 41 sequences were used after duplicate exclusion). To summarize, the N450 phylogeny presented herein contains two sequences not contained in the WGS inference.

Newly obtained N450 sequences were aligned with equivalent genome windows extracted from whole MeV B3 sequences (n=116 for entire set) obtained from NCBI, as was performed for WGS inference. Public repository accessions for sequences and sequencing data used in phylogenetic analyses is available in the study data repository at https://data.cdc.gov/Models/Measles-Case-and-Genetic-Metadata-Operation-Allies/b8tp-jsmh. Base substitution model for N450 was selected using the modeltest function of IQ-Tree v.2.1.2, [23] using the entire N450 segment, without partitioning. Recommended base substitution model was TN+F (BIC score: 2071·812). This substitution model was used to perform Bayesian tree inference as described above in common methods.

Identification of infector-infectee pairs and of unrelated patients

Three high confidence infector-infectee pairs (1→4, 3→8, and 30→28) were identified. Patients 1 and 4 were in Germany together before coming to the U.S., shared the same incoming international flight (Flight 3), as well as the same domestic flight (from Dulles International Airport (IAD) to Ft. McCoy), while patient 1 was infectious. Patients 3 and 8 shared the same barrack (Barrack B) at Ft. McCoy while patient 3 was

infectious and were the only two patients identified in that particular barrack. Patients 30 and 28 were members of the same family (Family 4) who traveled together from Spain to IAD (Flight 5) and onto Hotel A. The difference in days between the rash onsets of patients 1 and 4, 3 and 8, and 30 and 28 were 11, 9, and 11 days, respectively.

Six case pairs were known to be unrelated (1↠35, 24↠35, 25↠35, 30↠35, 31↠35, 47↠35). These pairs were used as a control set for genetic comparisons. Specifically, these cases were unambiguously known not to be part of the same measles virus transmission chain within the U.S.; i.e., they did not infect each other in the U.S. Case 35 was reported in MCB Quantico, was among the last few measles cases reported during OAW and was one of two patients who arrived via the Philadelphia International Airport (PHL). Cases 1, 24, 25, 30, 31, and 47 were reported in Ft. McCoy, Hotel A, and Ft. Pickett, were among the earliest cases reported during OAW, arrived via IAD, and had onset of rash >21 days before the rash onset of case 35.

Phylogenetic Analyses of N450 and WGS Windows

Context

Currently, surveillance of measles virus is performed by acquisition of partial-genome sequencing windows (N450 genotyping), and these sequences are universally analyzed across international surveillance networks to substantiate claims of measles elimination. Elimination is assigned a formal definition by WHO, specifying the absence of continuous transmission lasting greater than one year in the presence of a well-functioning surveillance system. [25] Since the diversity of circulating measles sequences is decreasing, post-elimination scenarios are envisioned in which multiple transmission chains would not be genetically distinguishable by N450, possibly leading to overestimates of transmission continuity. [26] Consequently, there is a perceived research need in the measles surveillance community to assess improvement to transmission chain discrimination offered by acquisition of WGS data, keeping in mind tradeoffs of expense inherent to implementation of WGS laboratory methods. [27,28] Resolution of phylogenetic models is expressed as a combination of (1) certainty of tree topology or grouping patterns, (2) certainty of molecular clock estimates, and (3) certainty of node dating when molecular clocks are used. We report improvements to these parameters in the study data (WGS) when compared to a model inferred from N450 only. Molecular surveillance of measles virus in Afghanistan is infrequently reported (94 sequences in MeaNS2 (who-gmrln.org/means2) 2011–present, accessed December 20, 2022), and so the dynamics of transmission within Afghanistan are poorly understood.

Posterior Statistics and Node Dating

N450 phylogeny was computed as described in supplemental methods (Fig. S6, S7). Mean N450 posterior clock rate was $5{\cdot}07 \times 10^{-3}$ substitutions/site/year (95% HPD Interval: $2{\cdot}56 \times 10^{-3} – 8{\cdot}07 \times 10^{-3}$). Mean N450 tree height (common ancestor age of entire B3 genotype tree, converted to calendar years) was 2010·090 (95% HPD Interval: 2007·782 – 2012·083). Mean common ancestor date of OAW specimens was 2020·549 (95% HPD Interval: 2019·883 – 2021·190).

WGS phylogeny was computed as described above in supplemental methods (Fig. 3). Mean posterior clock rate was $4{\cdot}98 \times 10^{-4}$ substitutions/site/year (95% HPD Interval: $4{\cdot}12 \times 10^{-4} – 5{\cdot}90 \times 10^{-4}$). Mean tree height (common ancestor age converted to calendar years) was 1993·288 (95% HPD Interval: 1997·484 – 1988·963). Mean common ancestor date of OAW specimens was 2015·408. (95% HPD Interval: 2014·157 – 2016·553).

Interpretation of Molecular Clocks

By contrast to the tree generated from WGS, resolution was lower for both (1) temporal basis (wider HPD intervals for node dating) and (2) tree topology (lower posterior node probabilities and fewer highly supported nodes (WGS: n=6, N450: n=4, at posterior>=0·9)). It is noteworthy that the 95% HPD intervals for molecular clock rates do not overlap for WGS and N450 inference as performed here. We interpret this to mean that, while a resolvable evolutionary process is observed when using only the partial N450 window, this inference artificially compresses the timescale of the true evolutionary rate of the virus, most likely a result of the exclusion of the considerable mutational evidence available in the noncoding regions. N450 is extensively used in surveillance because it is known to capture intra-type diversity of MeV but substitution rates (substitutions per site of sequence) for the entire N-L sequence, in this case, provide apparent evidence for more extensive conservation over time than are shown by N450.

Clock rates (substitutions per site per year) for measles virus are within those expected for respiratory viruses; for measles virus these rates are infrequently reported; previous studies are cited in the table below.

This study differs from previous work in several respects. First, specimens were exclusively from oropharyngeal or nasopharyngeal swab extracts, without intervening viral culture. Second, a metagenomic sequencing approach was used, meaning that read sets were produced without intervening PCR amplification. Lastly, a partitioned genetic model is implemented to infer separate base substitution rates from coding and noncoding genome regions. Current study is highlighted in gray.

Specimen Type	**Mean Clock Rate (Subs/Site/Year)**	**Phylogenetic Model Settings**	**Reference**
Oral fluids, cell culture isolate	$1{\cdot}8 \times 10^{-3}$ (N450) $6{\cdot}5 \times 10^{-3}$ (MF-NCR)	Base substitution: GTR Clock: Relaxed lognormal Constant population coalescent	Penedos 2015[28]
Cell culture isolate	$2{\cdot}32 \times 10^{-6}$ sub/site/generation	Base substitution: GTR Clock: Exponential population coalescent	Gardy 2015[27]
Lung Biopsy Throat Swab	$1{\cdot}15 \times 10^{-3}$ (N450) - B3 $1{\cdot}94 \times 10^{-3}$ (WGS) - B3	Base substitution: GTR Clock: Constant population coalescent	Penedos 2022[29]
Oral fluids/swab	$5{\cdot}07 \times 10^{-3}$ (N450) $4{\cdot}98 \times 10^{-4}$ (WGS/N-L span)	Base substitution: TIM+F+G4 (linked all CDS) TIM3+F+G4 (linked all NCR) Clock: Strict (both partitions) Skyline coalescent	Current Study

Interpretation of Topology

In both WGS and N450 trees, there is some topological uncertainty in the split of main clusters 1 and 3 (cluster 3 = single case) from cluster 2 (WGS posterior = 0·693, N450 posterior = 0·630), while support was somewhat higher for WGS. In both N450 and WGS trees, there was complete support (WGS posterior = 1·000, N450 posterior = 1·000) for the internal node representing the common ancestor of all OAW sequences and a closely related B3 strain sequenced in 2019, in California (MVs/California.USA/50·19[B3]). As mentioned, the resulting tree was observed to be better-resolved than that produced using the N450 Sanger windows. Considerable overlap of time intervals was observed for cluster-defining internal nodes in recent divergence of N450 sequences. We chiefly interpret these features to minimally support the existence of three circulating lineages predating importation to the United States with these evacuee cases. Comparison of N450 and WGS trees is shown in Fig. S7.

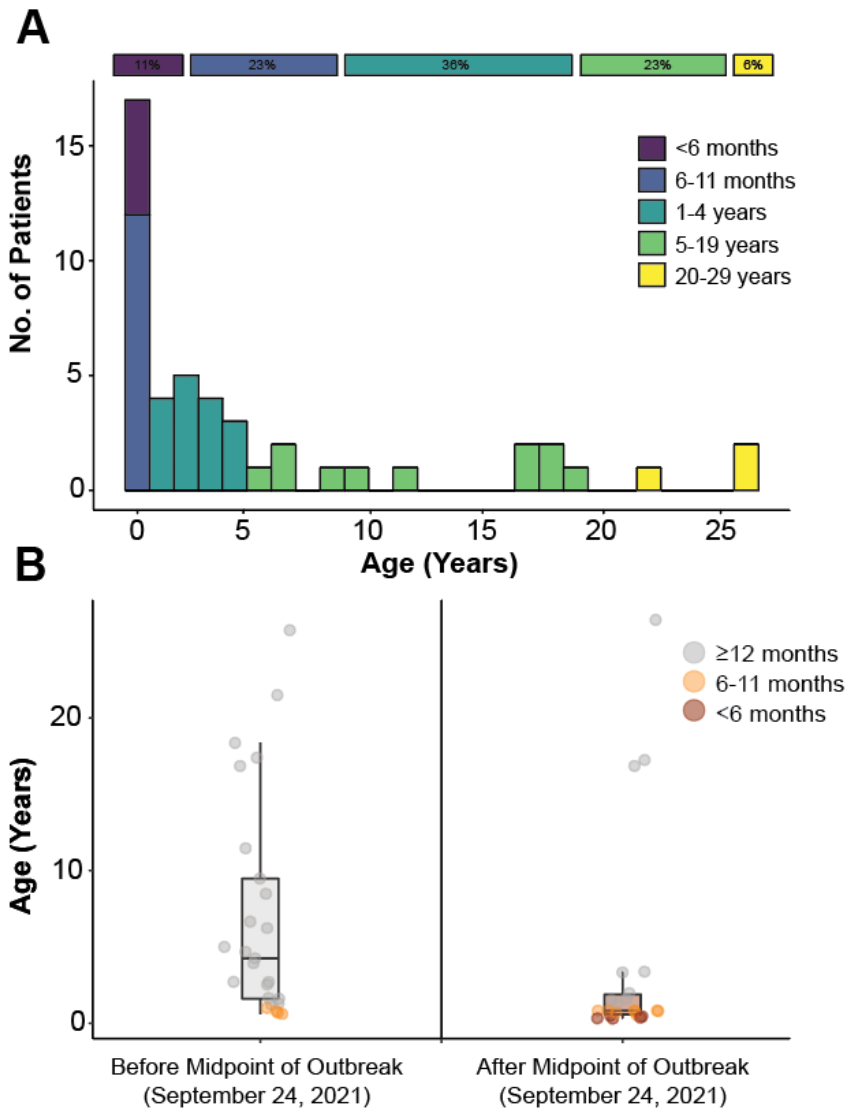

Figure S1. Age distribution of measles cases and change in age distribution before and after the midpoint of the outbreak during Operation Allies Welcome, August–October 2021.
Panel A shows a histogram of measles cases according to age in years, color-coded by age-group. The length of the horizontal bars is equivalent to the proportion of cases in each age-group category. Panel B shows the change in the age distribution of cases before and after the midpoint of the outbreak (September 24, 2021). Before September 24, 25 cases were reported, of which 21 (84%) occurred among those aged 12 months or older, 4 (16%) among those aged 6–11 months, and none among those aged <6 months. After September 24, 22 cases were reported, of which 9 (41%) occurred among those aged 12 months or older, 8 (36%) among those 6–11 months, and 5 (23%) among those aged <6 months.

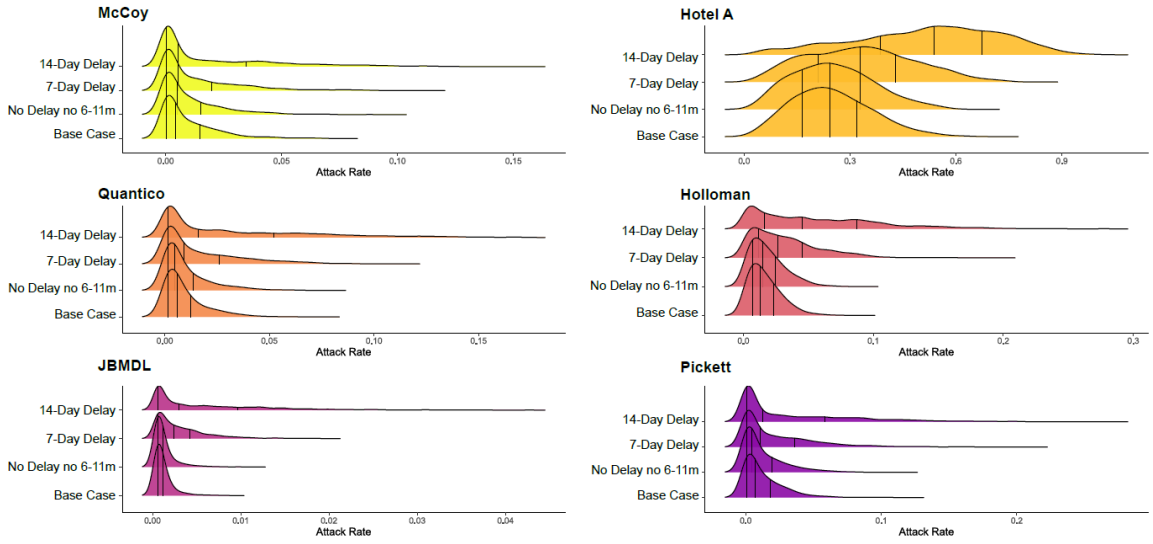

Figure S2. Location-specific measles attack rates under different vaccination scenarios.
Shown are density ridgeline plots of the measles attack rates at each of the five military bases (Ft. McCoy, MCB Quantico, Holloman Air Force Base, JB McGuire-Dix-Lakehurst, and Ft. Pickett), and the isolation and quarantine hotel, Hotel A, where measles cases were reported. In each panel, the base-case scenario (model results using vaccination uptake as it occurred) is compared to scenarios in which the age of MMR vaccine administration was not lowered to 6 months, vaccination was delayed 7 days, and vaccination was delayed 14 days. The vertical lines represent the 25th, 50th, and 75th quantiles.

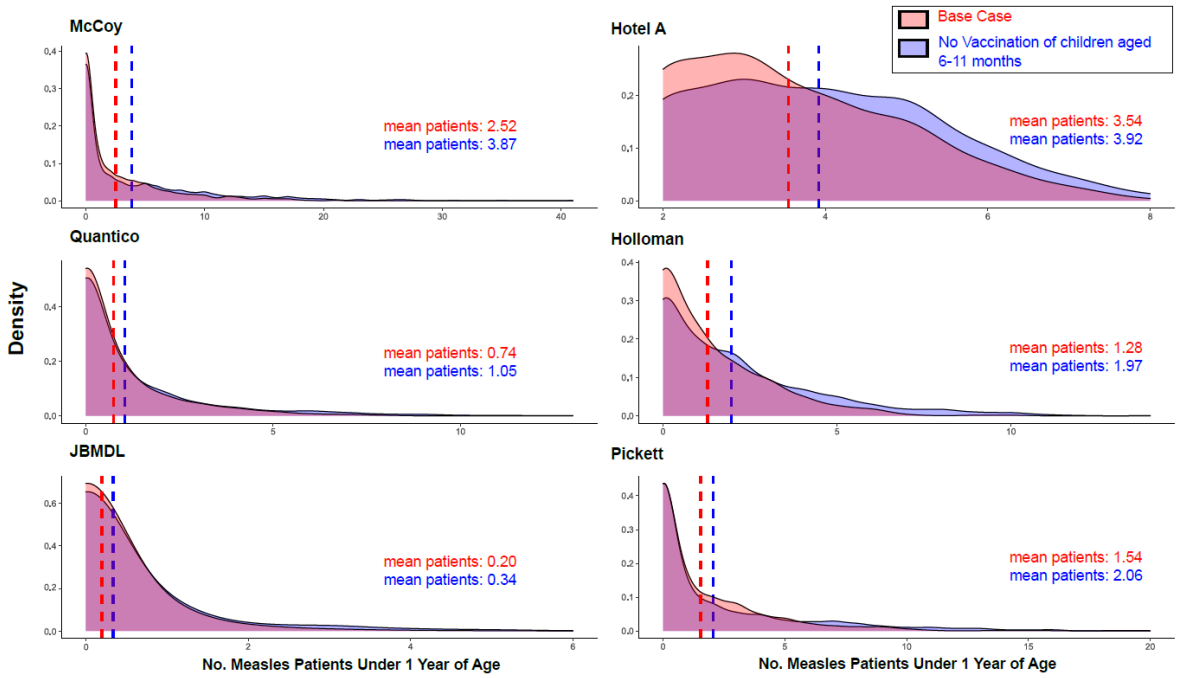

Figure S3. Location-specific number of measles cases aged less than one year in scenarios in which the age of MMR vaccine administration was and was not lowered to 6 months.

The distribution of the number of patients aged less than one year as predicted by the models are plotted comparing the base-case scenario (model results using MMR vaccination uptake as it occurred, which included infants aged 6–11 months) and a scenario in which infants aged 6–11 months were not vaccinated, at each of the five military bases and the isolation and quarantine hotel (Hotel A), where measles patients were reported. The red and blue vertical dashed lines represent the mean number of measles cases in the base case scenario and the no-vaccination scenario, respectively.

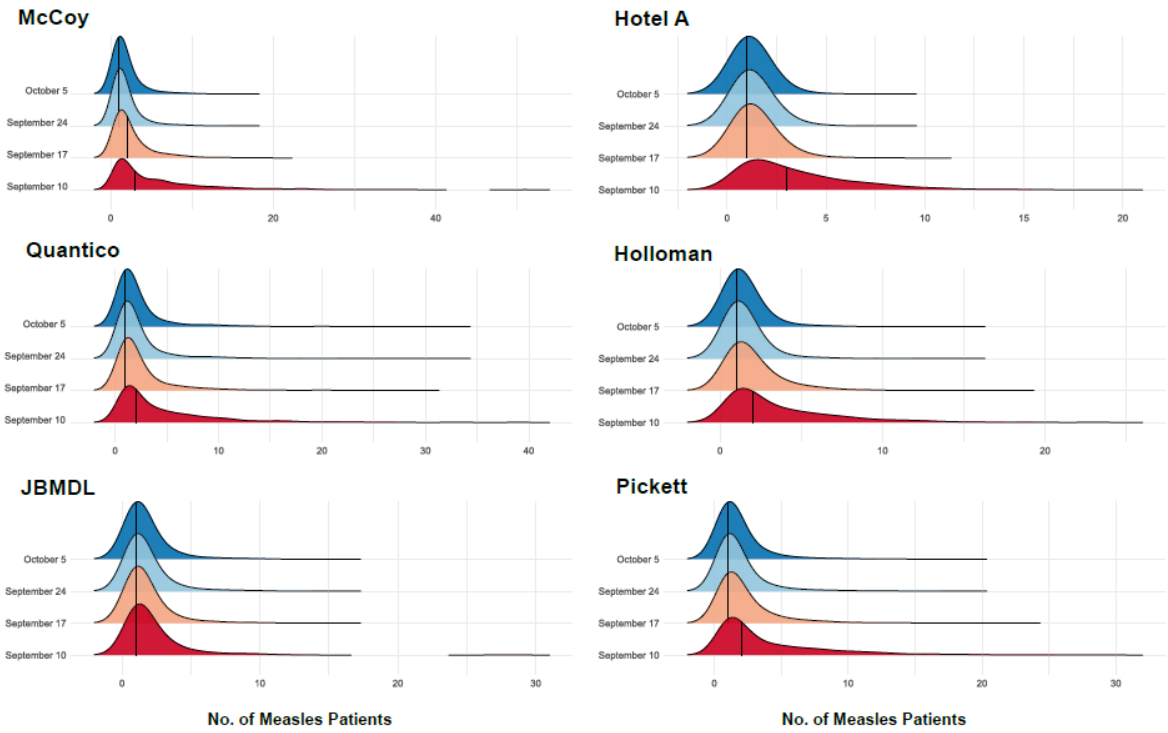

Figure S4. Location-specific number of measles cases in scenarios in which an additional importation occurred at different time points during the pause on incoming international flights.
Density ridgeline plots of the number of patients caused by a single additional importation arriving on September 10 (the day flights were paused), September 17 (one week later), September 24 (two weeks later), and October 5 (the day the flights resumed), at each of the five military bases and the isolation and quarantine hotel (Hotel A), where cases of measles were reported. The vertical lines represent the median.

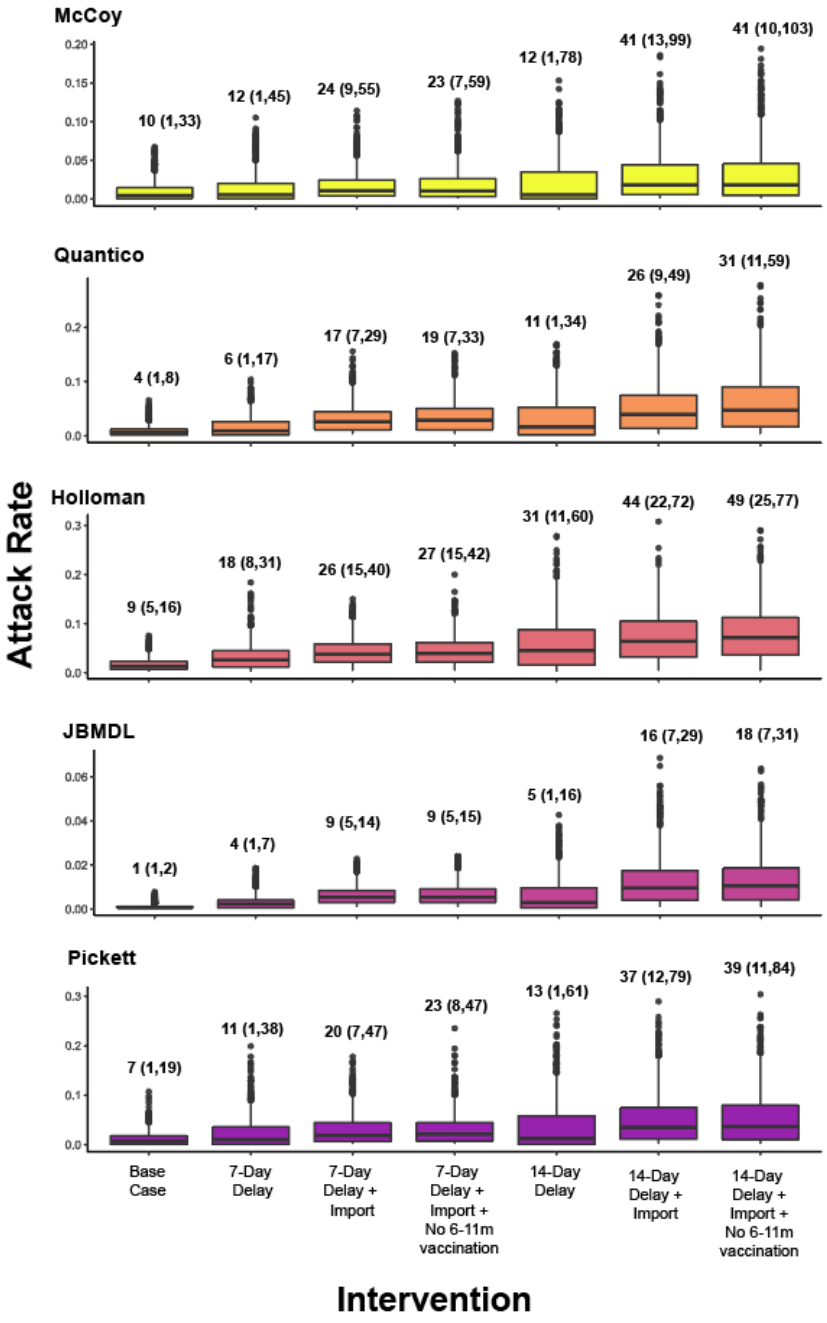

Figure S5. Location-specific measles attack rates under various combined intervention scenarios. At each of the five military bases where measles cases were reported, boxplots of measles attack rates as predicted by the model for different combinations of interventions are compared to the base-case scenario (interventions as they occurred). Combinations of interventions include a 7- or 14-day delay plus an additional importation on September 17 and/or not lowering the age of MMR vaccination to 6–11-months. The median number of measles cases and the interquartile range (IQR) are listed above each boxplot.

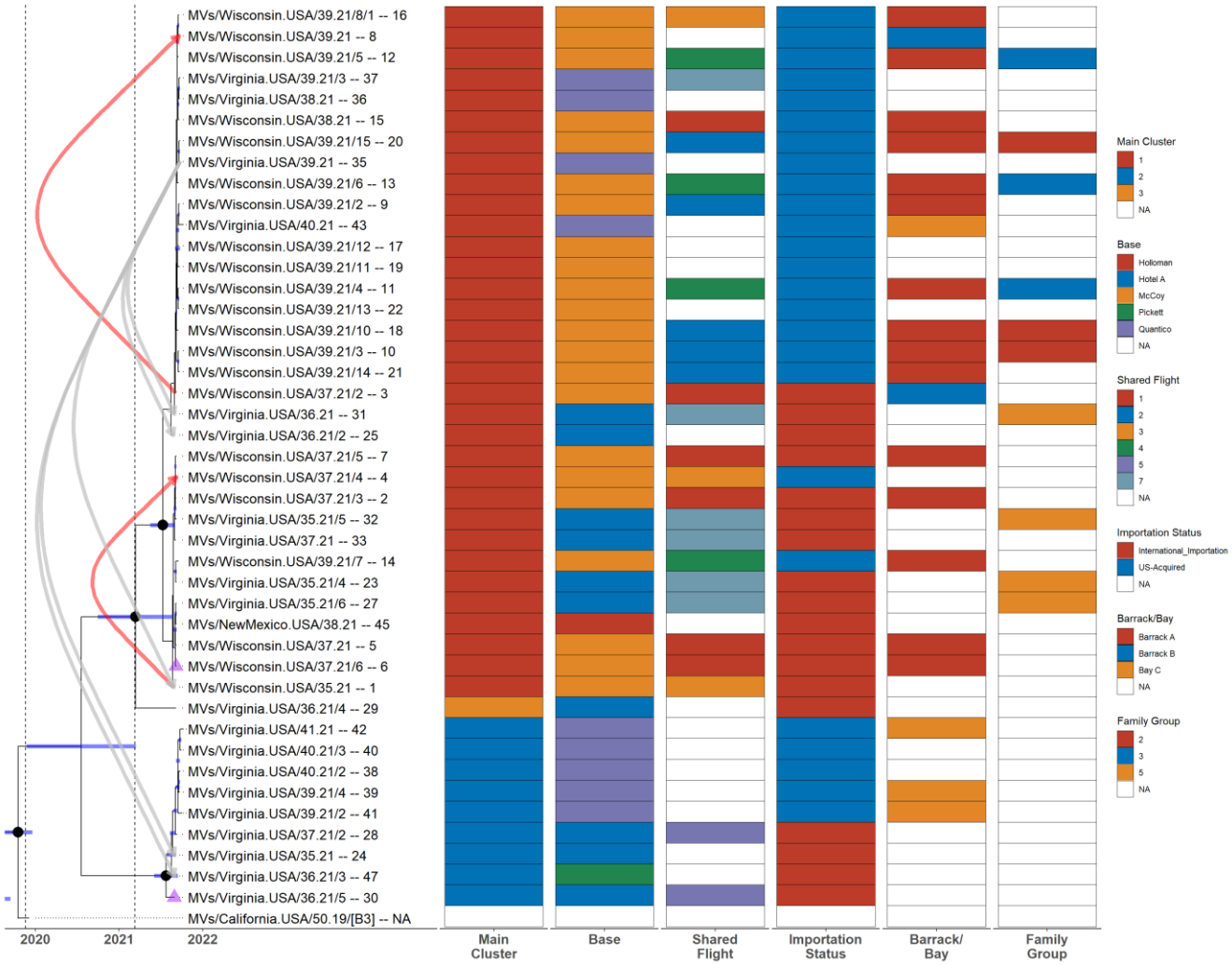

Figure S6. Phylogenetic Tree from N450 genotyping windows.
As shown in the main text for whole genome sequencing (Figure 5), the tree (leftmost) contains the inset group of the larger B3 tree with sequences obtained during Operation Allies Welcome study (n=43), with a closely related B3 strain (MVs/California.USA/50.19[B3]) shown for visual orientation. Metadata is shown as before for WGS (genetic cluster, arrival location, shared flight, importations status, barrack or bay, and family group). High-confidence transmission events are marked by red arrows and transmissions of nil-confidence are shown as grey arrows. Sequences for which N450 windows were available, but not included in the WGS tree are marked with a purple triangle on the branch tip. The time interval (95% HPD) for the origin of the common ancestor of all OAW specimens is shown with dashed lines for reference.

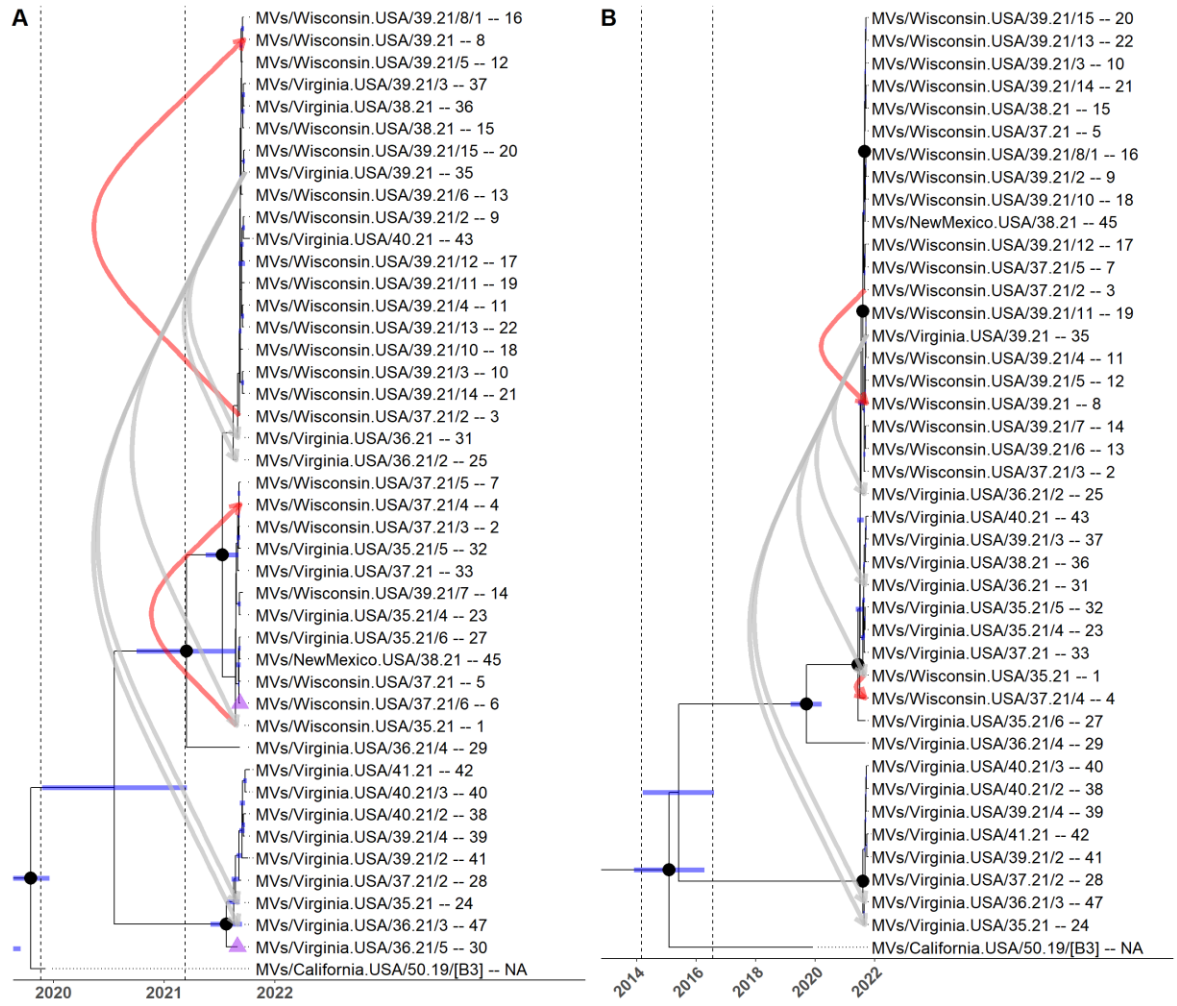

Figure S7. Comparison of measles virus genotype B3 phylogenies derived from N450 genotyping windows and WGS.

N450 (**A**) and WGS (**B**) subtrees (visualized as cutout from entire B3 set used in tree construction) are visualized for comparison of tree shape, node dating (purple bars), and certainty of tree shape (black dot is posterior >= 0·9). Trees are identical to those visualized in Fig S6 (N450) and Fig. 5 (WGS; main text). Briefly, (1) the temporal scale of the trees differs considerably, with wider date bars in N450 preventing discrimination of the cluster 1–2 divergence from that of 1 and 3; these dates are narrower in the WGS tree. (2) More internal nodes (n=6) exceed 0·9 posterior in the WGS result, with n=4 internal nodes supported at that level in the N450 phylogeny. Sequences available for N450 phylogenetic inference that were not available as WGS are denoted as purple triangles. In both panels, the time range (95% HPD) representing the common ancestor of all OAW specimens is shown with dashed vertical lines.

Table S1. Characteristics, outcomes, and testing results of 47 measles patients reported during Operation Allies Welcome, August–October 2021.

Variable	Value
Demographic characteristic	
Male sex — no. (%)	26 (55%)
Median age (range) — yr	1 (0–26)
Age distribution — no. (%)	
<6 mo	5 (11%)
6–11 mo	11 (23%)
1–4 yr	17 (36%)
5–19 yr	11 (23%)
20–29 yr	3 (6%)
Vaccination Status – no. (%)	
0 doses[a]	7 (15%)
1 dose	0 (0%)
2 doses	0 (0%)
Unknown	40 (85%)
Symptoms – no. (%)	
Fever[b]	44 (94%)
Generalized rash	47 (100%)
Cough	31 (66%)
Coryza	18 (38%)
Conjunctivitis	16 (34%)
Complications – no. (%)[c]	
Diarrhea, vomiting, and/or dehydration	25 (53%)
Otitis Media	3 (6%)
Pneumonia	3 (6%)
Any complication	26 (55%)
Outcomes – no. (%)	
Hospitalization	28 (60%)
Death	0 (0%)
Laboratory testing – no. (%)	
IgM-positive, RT-PCR-positive, or both	46 (98%)
IgM-positive alone	0 (0%)
RT-PCR-positive alone	33 (70%)
Both IgM-positive and RT-PCR-positive	13 (28%)

[a]Seven measles patients aged <9 months were classified as being unvaccinated as they were ineligible for routine measles–mumps–rubella (MMR) immunization in Afghanistan and the most recent supplementary immunization activity in Afghanistan occurred in 2018.
[b]Three measles patients in whom fever was not reported had generalized rash and were confirmed to have measles infection by RT-PCR.
[c]Complications are not mutually exclusive, some patients had more than one reported complication.

Table S2. Evaluation of a range of effectiveness of MMR vaccine campaign doses on model simulation results of measles attack rates and number of measles cases in five military bases with measles cases, under various scenarios, Operation Allies Welcome, August–October, 2021.

Scenario	Vaccine Effectiveness Assumption[a]					
	Base model		Lower		Upper	
	Median AR[b] (IQR) (%)	Median No. of Measles Cases (IQR)	Median AR (IQR)	Median No. of Measles Cases (IQR)	Median AR (IQR)	Median No. of Measles Cases (IQR)
Base Case	0·44 (0·12, 1·46)	27·6 (7·6, 92·0)	0·48 (0·12, 1·83)	30·0 (7·6, 115·5)	0·44 (0·10, 1·37)	27·6 (6·0, 86·6)
7-Day Delay	0·67 (0·15, 2·66)	42·0 (9·6, 168·0)	0·84 (0·15, 3·37)	53·1 (9·6, 212·7)	0·66 (0·15, 2·44)	41·7 (9·6, 153·9)
14-Day Delay	1·14 (0·15, 4·67)	72·1 (9·6, 294·2)	1·40 (0·15, 5·87)	88·4 (9·6, 370·0)	0·92 (0·15, 4·09)	57·8 (9·6, 257·7)
No vaccination of children aged 6–11 months	0·44 (0·10, 1·53)	27·6 (6·0, 96·3)	0·48 (0·12, 2·00)	30·3 (7·6, 126·1)	0·44 (0·10, 1·43)	27·6 (6·0, 90·1)
Additional importations to Ft. McCoy and Quantico[c]	0·76 (0·18, 2·00)	48·1 (11·4, 126·1)	0·89 (0·19, 2·57)	56·0 (12·0, 162·3)	0·75 (0·13, 1·83)	47·6 (8·4, 115·5

Abbreviations: VE, Vaccine Effectiveness; IQR, Inter-Quartile Range; AR, Attack Rate

[a]The base model assumes an effectiveness of MMR vaccine campaign doses of 84% for infants aged 6–11 months and 92·5% for persons aged ≥12 months. The lower and upper vaccine effectiveness assumptions use an effectiveness of MMR vaccine campaign doses of 72·0 for infants aged 6–11 months and 84·8% for persons aged ≥12 months, and 95·0% for infants aged 6–11 months and of 97·0% for persons aged ≥12 months, respectively. [14]

[b]Median and IQRs generated from 1,000 model simulations.

[c]Two additional importations, one at Ft. McCoy and one at MCB Quantico, on September 10.

Table S3. Evaluation of a range of R_0 values on model simulation results of measles attack rates and number of measles cases in five military bases with measles cases, under various scenarios, Operation Allies Welcome, August–October, 2021.

Scenario	R_0 Assumption[a]					
	R_0 of 14		Lower: R_0 of 5		Upper: R_0 of 18	
	Median AR[b] (IQR) (%)	Median No. of Measles Cases (IQR)	Median AR (IQR)	Median No. of Measles Cases (IQR)	Median AR (IQR)	Median No. of Measles Case (IQR)
Base Case	0·44 (0·12, 1·46)	27·6 (7·6, 92·0)	0·15 (0·06, 0·31)	9·6 (3·8, 19·3)	0·80 (0·12, 2·77)	50·4 (7·6, 174·9)
7-Day Delay	0·67 (0·15, 2·66)	42·0 (9·6, 168·0)	0·15 (0·10, 0·44)	9·6 (6·0, 27·6)	1·61 (0·24, 5·84)	101·2 (15·2, 368·2)
14-Day Delay	1·14 (0·15, 4·67)	72·1 (9·6, 294·2)	0·18 (0·10, 0·44)	11·2 (6·0, 27·6)	3·10 (0·29, 12·13)	195·4 (18·4, 764·7)
No vaccination of children aged 6–11 months	0·44 (0·10, 1·53)	27·6 (6·0, 96·3)	0·15 (0·06, 0·31)	9·6 (3·8, 19·3)	0·76 (0·12, 3·11)	48·1 (7·6, 195·9)
Additional importations to Ft. McCoy and Quantico[c]	0·76 (0·18, 2·00)	48·1 (11·4, 126·1)	0·29 (0·10, 0·44)	18·0 (6·0, 28·9)	1·46 (0·19, 3·66)	92·4 (12·0, 231·0)

Abbreviations: VE, Vaccine Efficacy; IQR, Inter-Quartile Range, AR, Attack Rate

[a]The base model assumes a R_0 of 14 based on estimates of the effective reproduction number R_e and the proportion of the population that was susceptible. The upper and lower R_0 used in these analyses were based on a range of previously published R_0 estimates for measles in various settings. [8,9]

[b]Median and IQRs generated from 1,000 model simulations

[c]Two additional importations, one at Ft. McCoy and one at MCB Quantico, on September 10.

Table S4. Evaluation of a range of population susceptibility values on model simulation results of measles attack rates and number of measles cases in five military bases with measles cases, under various scenarios, Operation Allies Welcome, August–October, 2021.

Scenario	Susceptibility Assumption					
	Baseline		Susceptibility increased by 10%		Susceptibility decreased by 10%	
	Median AR[a] (IQR) (%)	Median No. of Measles Cases (IQR)	Median AR (IQR)	Median No. of Measles Cases (IQR)	Median AR (IQR)	Median No. of Measles Cases (IQR)
Base Case	0·44 (0·12, 1·46)	27·6 (7·6, 92·0)	0·42 (0·11, 1·65)	29·4 (7·6, 114·2)	0·34 (0·11, 1·30)	19·2 (6·0, 73·5)
7-Day Delay	0·67 (0·15, 2·66)	42·0 (9·6, 168·0)	0·82 (0·14, 3·18)	56·9 (9·6, 220·6)	0·59 (0·17, 2·20)	33·6 (9·6, 125·0)
14-Day Delay	1·14 (0·15, 4·67)	72·1 (9·6, 294·2)	1·39 (0·14, 5·94)	96·1 (9·6, 411·9)	0·81 (0·17, 3·56)	46·0 (9·6, 201·9)
No vaccination of children aged 6–11 months	0·44 (0·10, 1·53)	27·6 (6·0, 96·3)	0·52 (0·11, 1·82)	36·1 (7·6, 126·2)	0·40 (0·11, 1·38)	22·8 (6·0, 78·1)
Additional importations to Ft. McCoy & Quantico[b]	0·76 (0·18, 2·00)	48·1 (11·4, 126·1)	0·83 (0·16, 2·22)	57·6 (11·4, 154·0)	0·68 (0·15, 1·73)	38·5 (8·4, 97·9)

Abbreviations: VE, Vaccine Efficacy; IQR, Inter-Quartile Range, AR, Attack Rate

[a] Median and IQRs generated from 1,000 model simulations

[b]Two additional importations, one at Ft. McCoy and one at MCB Quantico, on September 10.

Table S5. Base substitution (WGS hamming distance) for relevant exposure groups. For each exposure group, accumulation of base substitutions is depicted in reference to the first ordinal case (green).

		Ordinal Case Number																																														
Exposure Type	**Exposure Group**	**1**	**2**	**3**	**4**	**5**	**6**	**7**	**8**	**9**	**10**	**11**	**12**	**13**	**14**	**15**	**16**	**17**	**18**	**19**	**20**	**21**	**22**	**23**	**24**	**25**	**26**	**27**	**28**	**29**	**30**	**31**	**32**	**33**	**34**	**35**	**36**	**37**	**38**	**39**	**40**	**41**	**42**	**43**	**44**	**45**	**46**	**47**
Family Group	A										0								2		1																											
	B											0	0	0																																		
	C																							0				3				0	0															
Shared Flight	E		0	1		2		1								2																																
	F									0	1								1		0	0																										
	G	0			2												2																															
	M											0	0	0	1																																	
	O																							0				3				0	0	0				0										
	R																												0																			
Importation Status	International I.	0	2	1		2		1																0	104	1		3	104	35		0	0	0												2		104
	US-Acquired				0				3	4	5	3	3	3	4	4	4	4	5	3	4	4	4													3	2	2	106	106	106	106	106	3				
Shared Barrack	Barrack A		0			2		1		2	3	1	1	1	2	2	2		3		2	2																										
	Barrack B			0					0																																							
	Bay A																																							0		0	0	105				
Infector-Infectee Pairs	1,4	0			2																																											
	3,8			0					0																																							
Unrelated Cases	1,35	0																																		1												
	24,35																								0											105												
	25,35																									0										2												
	31,35																															0				1												

Table S6. Base substitution (N450 hamming distance) for relevant exposure groups. For each exposure group, accumulation of base substitutions is depicted in reference to the first ordinal case (green).

		Ordinal Case Number																																														
Exposure Type	**Exposure Group**	**1**	**2**	**3**	**4**	**5**	**6**	**7**	**8**	**9**	**10**	**11**	**12**	**13**	**14**	**15**	**16**	**17**	**18**	**19**	**20**	**21**	**22**	**23**	**24**	**25**	**26**	**27**	**28**	**29**	**30**	**31**	**32**	**33**	**34**	**35**	**36**	**37**	**38**	**39**	**40**	**41**	**42**	**43**	**44**	**45**	**46**	**47**
Family Group	A										0								0		0																											
	B											0	0	0																																		
	C																							0				0				0	0															
Shared Flight	E		0	0		0	0	0								0																																
	F									0	0								0		0	0																										
	G	0			0												0																															
	M											0	0	0	0																																	
	O																							0				0				0	0	0				0										
	R																												0		0																	
Importation Status	International I.	0	0	0		0	0	0																0	7	0		0	7	3	7	0	0	0												0		7
	US-Acquired				0				0	0	0	0	0	0	0	0	0	0	0	0	0	0	0													0	0	0	7	7	7	7	7	0				
Shared Barrack	Barrack A		0			0	0	0		0	0	0	0	0	0	0	0		0		0	0																										
	Barrack B			0					0																																							
	Bay A																																							0		0	0	7				
Infector-Infectee Pairs	1,4	0			0																																											
	3,8			0					0																																							
	30,28																												0		0																	
Unrelated Cases	1,35	0																																		0												
	24,35																								0											7												
	25,35																									0										0												
	30,35																														0					7												
	31,35																															0				0												

Table S7. Public repository accessions for sequences and sequencing data used in phylogenetic analyses. Table is available in the study data repository at https://data.cdc.gov/Models/Measles-Case-and-Genetic-Metadata-Operation-Allies/b8tp-jsmh**.**

Supplementary References

1. Roy F, Mendoza L, Hiebert J, et al. Rapid Identification of Measles Virus Vaccine Genotype by Real-Time PCR. *J Clin Microbiol* 2017; **55**(3): 735-43.
2. Cao Y, Gillespie DT, Petzold LR. Adaptive explicit-implicit tau-leaping method with automatic tau selection. *J Chem Phys* 2007; **126**(22): 224101.
3. Johnson P. adaptivetau: Efficient Stochastic Simulations in R. 2014 2014. https://cran.r-project.org/web/packages/adaptivetau/vignettes/adaptivetau.pdf. (accessed September 28, 2021.
4. Gastanaduy PA, Funk S, Lopman BA, et al. Factors Associated With Measles Transmission in the United States During the Postelimination Era. *JAMA Pediatr* 2020; **174**(1): 56-62.
5. Wallinga J, Teunis P. Different epidemic curves for severe acute respiratory syndrome reveal similar impacts of control measures. *Am J Epidemiol* 2004; **160**(6): 509-16.
6. Cori A, Ferguson NM, Fraser C, Cauchemez S. A new framework and software to estimate time-varying reproduction numbers during epidemics. *Am J Epidemiol* 2013; **178**(9): 1505-12.
7. Klinkenberg D, Nishiura H. The correlation between infectivity and incubation period of measles, estimated from households with two cases. *J Theor Biol* 2011; **284**(1): 52-60.
8. Anderson R, May R. Infectious Diseases of Humans: Dynamics and Control. New York, NY: Oxford University Press; 1991.
9. Guerra FM, Bolotin S, Lim G, et al. The basic reproduction number (R0) of measles: a systematic review. *Lancet Infect Dis* 2017; **17**(12): e420-e8.
10. Thompson RN, Stockwin JE, van Gaalen RD, et al. Improved inference of time-varying reproduction numbers during infectious disease outbreaks. *Epidemics* 2019; **29**: 100356.
11. Yang W. Transmission dynamics of and insights from the 2018-2019 measles outbreak in New York City: A modeling study. *Sci Adv* 2020; **6**(22): eaaz4037.
12. Keeling MJ, Grenfell BT. Understanding the persistence of measles: reconciling theory, simulation and observation. *Proc Biol Sci* 2002; **269**(1489): 335-43.
13. McLean HQ, Fiebelkorn AP, Temte JL, Wallace GS, Centers for Disease C, Prevention. Prevention of measles, rubella, congenital rubella syndrome, and mumps, 2013: summary recommendations of the Advisory Committee on Immunization Practices (ACIP). *MMWR Recomm Rep* 2013; **62**(RR-04): 1-34.
14. Uzicanin A, Zimmerman L. Field effectiveness of live attenuated measles-containing vaccines: a review of published literature. *J Infect Dis* 2011; **204 Suppl 1**: S133-48.
15. World Health Organization DoI, Vaccines, and Biologicals (IVB). Meeting of the Advisory Committee on Immunization and Vaccines related Implementation Research (IVIR-AC). August 2021 2021. http://terrance.who.int/mediacentre/data/sage/210907-IVIR-AC-Pink-Book-August2021.pdf (accessed July 18, 2022.
16. Goodson JL, Teleb N, Ashmony H, et al. Progress Toward Measles Elimination - Eastern Mediterranean Region, 2013-2019. *MMWR Morb Mortal Wkly Rep* 2020; **69**(15): 439-45.

17. Guerra FM, Crowcroft NS, Friedman L, et al. Waning of measles maternal antibody in infants in measles elimination settings - A systematic literature review. *Vaccine* 2018; **36**(10): 1248-55.

18. Freidl GS, Tostmann A, Curvers M, et al. Immunity against measles, mumps, rubella, varicella, diphtheria, tetanus, polio, hepatitis A and hepatitis B among adult asylum seekers in the Netherlands, 2016. *Vaccine* 2018; **36**(12): 1664-72.

19. Bankamp B, Byrd-Leotis LA, Lopareva EN, et al. Improving molecular tools for global surveillance of measles virus. *J Clin Virol* 2013; **58**(1): 176-82.

20. Metsky HC, Siddle KJ, Gladden-Young A, et al. Capturing sequence diversity in metagenomes with comprehensive and scalable probe design. *Nat Biotechnol* 2019; **37**(2): 160-8.

21. Bouckaert R, Vaughan TG, Barido-Sottani J, et al. BEAST 2.5: An advanced software platform for Bayesian evolutionary analysis. *PLoS Comput Biol* 2019; **15**(4): e1006650.

22. Drummond AJ, Rambaut A, Shapiro B, Pybus OG. Bayesian coalescent inference of past population dynamics from molecular sequences. *Mol Biol Evol* 2005; **22**(5): 1185-92.

23. Minh BQ, Schmidt HA, Chernomor O, et al. IQ-TREE 2: New Models and Efficient Methods for Phylogenetic Inference in the Genomic Era. *Mol Biol Evol* 2020; **37**(5): 1530-4.

24. Russel PM, Brewer BJ, Klaere S, Bouckaert RR. Model Selection and Parameter Inference in Phylogenetics Using Nested Sampling. *Syst Biol* 2019; **68**(2): 219-33.

25. Monitoring progress towards measles elimination. *Wkly Epidemiol Rec* 2010; **85**(49): 490-4.

26. Brown KE, Rota PA, Goodson JL, et al. Genetic Characterization of Measles and Rubella Viruses Detected Through Global Measles and Rubella Elimination Surveillance, 2016-2018. *MMWR Morb Mortal Wkly Rep* 2019; **68**(26): 587-91.

27. Gardy JL, Naus M, Amlani A, et al. Whole-Genome Sequencing of Measles Virus Genotypes H1 and D8 During Outbreaks of Infection Following the 2010 Olympic Winter Games Reveals Viral Transmission Routes. *J Infect Dis* 2015; **212**(10): 1574-8.

28. Penedos AR, Myers R, Hadef B, Aladin F, Brown KE. Assessment of the Utility of Whole Genome Sequencing of Measles Virus in the Characterisation of Outbreaks. *PLoS One* 2015; **10**(11): e0143081.

29. Penedos AR, Fernandez-Garcia A, Lazar M, Ralh K, Williams D, Brown KE. Mind your Ps: A probabilistic model to aid the interpretation of molecular epidemiology data. *EBioMedicine* 2022; **79**: 103989.